IOPscience iopscience.iop.org

Home Search Collections Journals About Contact us My IOPscience

Indium-impurity interactions in a nickel host

This article has been downloaded from IOPscience. Please scroll down to see the full text article.

1991 J. Phys.: Condens. Matter 3 7575

(http://iopscience.iop.org/0953-8984/3/39/004)

View the table of contents for this issue, or go to the journal homepage for more

Download details:
IP Address: 171.66.16.147
The article was downloaded on 11/05/2010 at 12:35

Please note that terms and conditions apply.

J. Phys.: Condens. Matter 3 (1991) 7575–7586. Printed in the UK

Indium–impurity interactions in a nickel host

P Decoster†, G De Donckert†, M Rots† and A Z Hrynkiewicz‡
† Instituut voor Kern- en Stralingsfysika, Katholieke Universiteit Leuven, B-3001 Leuven, Belgium
‡ H Niewodniczanski Institute of Nuclear Physics, Cracow, Poland

Received 30 January 1991, in final form 13 May 1991

Abstract. The electric field gradients created at ^{111}Cd nuclei by dilute Al, V and Cr impurities in the nickel matrix are studied by the technique of time-differential perturbed angular correlation. The results show conclusively that there exists a strong repulsive interaction between the In probe and the Al, V or Cr impurity atoms. The magnetic hyperfine field satellites due to various probe–impurity configurations originate from a highly non-random distribution of impurities within a 78-atom sphere (five atomic shells in a FCC lattice) around the In probe.

1. Introduction

In a search for magnetic satellite hyperfine fields in dilute ferromagnetic alloys and their relation to atomic short-range ordering, we studied the Ni–X (X ≡ Al, V, Cr, ...) system by perturbed-angular-correlation (PAC) spectroscopy using the familiar ^{111}Cd probe. For many years, experimental efforts were directed towards an understanding of the disturbance around an impurity in a metal host. Ever since the discovery [1] of large hyperfine fields at impurities in ferromagnetic hosts, a great deal of work was concentrated on hyperfine field studies by both spin–echo NMR [2] and Mössbauer techniques [3]. Because the magnetic disturbance induced by an impurity should be reflected in the hyperfine field, these studies are complementary to probing the spatial variation of local magnetization by neutron scattering techniques. Oscillations in the conduction electron polarization (CEP) of the RKKY type are generally accepted to be manifested by hyperfine field shifts which are positive as well as negative relative to the pure matrix value. Whenever those satellites could be observed, assignment to a specific near-neighbour configuration was often doubtful because of existing deviations from randomness in the dilute binary alloy. Only results from ordered DO_3-type alloys [4] turn out to be interpretable in a convincing manner. Highly valuable data are those which make it possible to differentiate, rather in a model-independent way, between the different neighbour contributions to the hyperfine field. Two essential conditions should be fulfilled: substantial but well-defined hyperfine field shifts and objective criteria to define the influence sphere around the probe. Both determine the variety of relevant impurity configurations and corresponding satellite amplitudes. Most probably the need for an additional impurity as probe explains why PAC spectroscopy appears so scarcely in the near-neighbour interaction literature. Moreover the near insolubility

0953-8984/91/397575 + 12 $03.50 © 1991 IOP Publishing Ltd

of indium in iron excludes the use of the familiar PAC probe to study the iron-based alloys. In this paper we present a case where surprisingly the microscopic tendency for impurity repulsion was helpful in the identification of hyperfine field satellites.

2. Sample preparation

The time-differential perturbed-angular-correlation (TDPAC) [5] experiments were performed through the 173–247 keV $\gamma\gamma$ sequence in the decay of the ^{111}In to ^{111}Cd nucleus. The aim was to measure, above the Curie temperature T_C the hyperfine interaction of the quadrupole moment of the 247 keV state (lifetime $\tau = 123$ ns) with the internal electric field gradient (EFG) produced by the impurities in the Ni lattice, and below T_C, 633 K, the magnetic hyperfine field distribution sensed at the ^{111}Cd probe.

The samples were produced in the following way: the Ni–Al, Ni–V and Ni–Cr solid solutions with concentration c up to 2.5 at.% were prepared from 99.999% purity constituents by melting in an induction furnace under Ar atmosphere, after evacuation to better than 10^{-6} Torr. The radioactive carrier-free $^{111}InCl_3$ was deposited on the rolled alloy foil and the foil was remelted under an Ar atmosphere, thereby introducing the ^{111}In probe as a tracer into the lattice. All samples were annealed for some hours under a H_2 atmosphere at 1173 K. Thus our samples contain three elements, the host, the solute impurity atoms X (X ≡ Al, V, Cr) and the very dilute radioactive ^{111}In atoms, which decay to ^{111}Cd, the nucleus used as a probe in the TDPAC experiments. After thermal treatment the sample was cooled very slowly to room temperature. The series of Ni-based solid solutions investigated in this study were all of the substitutional type. The concentration and homogeneity of each alloy were checked by means of x-ray microprobing.

For each impurity the electric quadrupole interaction was measured just above 633 K, the Curie temperature, in a resistance furnace under vacuum conditions, with a temperature controller giving a stability of about 2 K. All magnetic interaction measurements were performed at room temperature.

3. Experimental set-up and data analysis

The angular correlation apparatus is a conventional fast–slow coincidence set-up with four NaI(Tl) detectors. The time resolution was better than 2.5 ns. In view of the fact that we are interested in observing small amplitude effects due to the nearest-neighbour contributions to the hyperfine field, it was essential to perform the room-temperature experiments, with high statistics. In our spectra the number of coincidences at $t = 0$ was at least 5×10^4.

The time-dependent correlation anisotropy $R(t)$ is calculated as usual using the expression

$$R(t) = [W_{AC}(\pi, t)/W_{AD}(\pi/2, t)][W_{BD}(\pi, t)/W_{BC}(\pi/2, t)] - 1 \qquad (1)$$

where for example $W_{AC}(\pi, t)$ represents the coincidence counting rate at an angle of

180° between detectors labelled A and C. This anisotropy can be expressed for a randomly oriented static interaction in a polycrystalline sample as follows:

$$R(t) = A\left(a_0 + \sum_n a_n \cos(\omega_n t)\exp(-\delta\omega_n t)\right) \tag{2}$$

assuming a Lorentzian distribution $\delta\omega_n$ of the interaction frequency ω_n. The anisotropy A is well known and solely determined by detector geometry as well as characteristics of the nuclear decay.

For a static, randomly oriented, axially symmetric electric quadrupole interaction the interaction frequencies are harmonics; thus $\omega_n = n\omega_0$ with $n = 1, 2, 3$ and the amplitudes a_n are well known constants;

$$\omega_0 = 6\omega_Q \qquad \omega_Q = eQV_{zz}/\hbar 4I(2I-1)$$

where, for ^{111}Cd, the nuclear spin $I = \frac{5}{2}$, the nuclear quadrupole moment in the intermediate state of $\gamma\gamma$ cascade is $Q = +0.83(2)b$ and V_{zz} is the magnitude of the axial EFG. In those cases where the EFG is non-axially symmetric the harmonicity of the frequency components is lost.

In the case of a static magnetic dipole interaction,

$$R(t) = A\left(a_0 + \sum_n a_n \cos(\omega_n t)\exp(-\delta\omega_n t)\right)$$

where $\omega_n = n\omega_B$ (with $n = 1, 2$) and $\omega_n = 2\pi\nu_n$ contains

$$\nu_B = \mu B/Ih = (-2.33250)B \text{ MHz}$$

the Larmor precession frequency in a magnetic hyperfine field B T, for the case of ^{111}Cd with $\mu = -0.7650(25)\mu_N$ in its $I = \frac{5}{2}$ state at 247 keV. Again the frequency amplitudes a_n are known constants.

Finally, we remark that, for each of the possible microscopic environments of the probe an expression such as equation (2) contributes to the complete experimental $R(t)$-function. A particular probe–impurity configuration is identified by the ν_n-frequency set and their distribution widths $\delta\nu_n$. The probability of forming this configuration (referred to as 'sites') is given by the relative amplitudes corresponding to the frequency set. Probe atoms at substitutional lattice sites in a perfect FCC nickel environment experience a cubic charge distribution and therefore no electric quadrupole interaction is detected. We refer to this configuration as the 'cubic fraction', which contributes a constant to the $R(t)$-function.

4. Results

4.1. Quadrupole interaction results

Just above the Curie temperature, two sites could be identified in all the investigated nickel-based alloys; a fraction f_1 of the probes subjected to a distribution of interaction frequencies centred around a low value ω_1, while a second part $f_0 = 1 - f_1$ experiences no hyperfine interaction (cubic fraction) and therefore contributes a constant to the expression for $R(t)$.

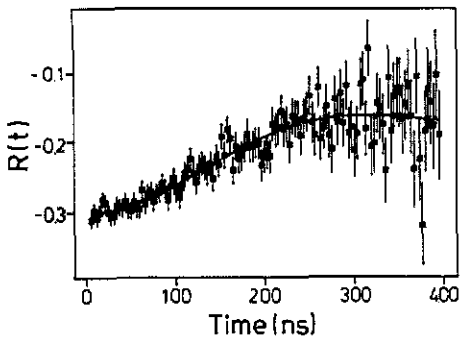

Figure 1. Typical quadrupole spectrum illustrating a strong repulsive probe–impurity interaction (^{111}In–$Ni_{97.7}Cr_{2.3}$ at 663 K).

Table 1. Comparison of the quadrupole interaction strength and corresponding cubic fraction f_0 measured for different impurities in dilute Ni alloys at the ^{111}In probe ($T > T_C = 633$ K).

Impurity	System	Measurement temperature (K)	eQV_{zz}/h (MHz)	$\delta\omega$ (MHz)	Cubic fraction f_0 (%)
V	$Ni_{0.997}V_{0.003}$	673	3.7(5)	—	79(4)
Al	$Ni_{0.986}Al_{0.014}$	663	2.94(4)	—	43(1)
Cr	$Ni_{0.977}Cr_{0.023}$	663	5.1(2)	—	55(1)

A typical result for the experimental anisotropy factor $R(t)$ is shown in figure 1. The full curve in the figure shows the result of the least-squares fitting of the two-site expression, based on equation (2), to the data. The results displayed in table 1 were obtained, assuming that probes belonging to the non-cubic fraction f_1 sense a finite interaction strength without any distribution. In view of the small value for the frequency and the limited time region measured, other approaches are possible. Therefore fitting was also done assuming that the fraction f_1 of probes experience a Gaussian distribution $\delta\omega$ around zero frequency. These two approaches result in essentially comparable quality, giving only a small change in the fractions f_1 and f_0.

The amount of constant anisotropy (f_0, cubic fraction) reflects the fraction of probes located in an environment of pure nickel. The rest of the probes experience a very weak quadrupole interaction strength eQV_{zz}/h, independent of the alloy concentration. A well defined quadrupole interaction strength of at least 15–20 MHz, expected for InX first-nearest-neighbour close pairs in FCC lattices [6, 7] and seen in nickel for the Ni–Rh(In) [8] case, is obviously not observed here.

In the case of a repulsive probe–impurity interaction the probe atom prefers to be surrounded by host atoms, rather than by the impurity atoms X. The probability to find an impurity in a neighbouring shell is thus smaller than expected for a random impurity distribution over the alloy. It is well known that the quadrupole interaction depends as r^{-3} on the probe–impurity distance. Therefore one generally infers from the short-range sensitivity of the quadrupole interaction that defects (impurities) beyond the second-nearest-neighbour shell contribute to the TDPAC spectrum with a distribution around an interaction frequency close to zero or even by simply a constant.

Furthermore, in first approximation, the point charge model for the EFG predicts a quadrupole interaction frequency reduction according to 1:0.35:0.19:0.13:0.09 in going from the first-nearest-neighbour probe–impurity pair to the fifth-nearest-neighbour pair. Extrapolating the measured first-neighbour interaction of 30 MHz [8], we expect a $eQV_{zz}/h \simeq 11$ MHz, the frequency for the second-nearest-neighbour InX pair, definitely not observed in our spectra. On the contrary, the low value for eQV_{zz}/h as given in table 1 may well be associated with the interaction frequency expected for distant probe–impurity pairs. We return to this point in the discussion.

Thus our quadrupole interaction measurements indicate that Al, V and Cr impurities in the nickel lattice are repelled by the In probe atoms and located beyond the first-nearest-neighbour shells around indium. The repulsive interaction is strong and the corresponding interaction energy B appears in an Arrhenius temperature dependence [6] as $\exp(-B/kT)$, is certainly higher than 100 meV, because at 663 K the presence of In–impurity nearest-neighbour pairs is not observed.

This repulsive In–X near-neighbour interaction observed here is further confirmed by the following: impurity–impurity interactions in ternary dilute alloys, studied by Krolas [9], reveal that the heat of solution of the bulk materials, constituting the alloy, can be used to predict the nature of the probe–impurity interaction. On this basis, one expects indeed a strong repulsive first-nearest-neighbour In–Al, In–V and In–Cr interaction in nickel. The X–X interaction of the impurity atoms between themselves, estimated using the Krolas [9] model, is also repulsive. It is strongest for Al and weakest for Cr atoms.

In conclusion, the quadrupole interaction measured in the paramagnetic phase of Ni–X dilute alloys strongly indicate that no In–X (X = Al, V, Cr) close pairs are formed, but rather indium repels those impurities beyond at least the second-nearest-neighbour shell. It should be mentioned that the interaction of In with other impurities in nickel is found to be different. For instance In attracts Pd impurities, while Rh impurities are weakly repelled [8]. On the other hand, our recent work suggests that In does not influence the random distribution of Fe and Co impurities in the Ni lattice.

4.2. Results on the magnetic hyperfine interaction

Subsequently, after the samples had been annealed for 36 h at 663 K (while measuring the quadrupole spectra), the samples were cooled slowly to room temperature. In figure 2 we show the results for Ni–Al as functions of both time and frequency. The time spectrum (figure 2(*a*)) results from the procedure summarized in equation (1) and represents the nuclear spin precession under the influence of a magnetic hyperfine field. Before fitting these data according to equation (2), we calculate the Fourier transform, given in figure 2(*c*) in order to reveal the different frequency components. From these two types of spectrum shown in figure 2, we may already subtract the main features. Clearly satellite hyperfine fields are present, indicated

(i) by the asymmetric frequency distribution in the Fourier transform spectrum,

(ii) by the damping of the correlation anisotropy as a function of time and

(iii) by the change in the structure of the spin precession pattern (misfit in figure 2(*a*)).

In addition a phase mismatch results from a fitting of the time spectrum with equation (2) adapted for the magnetic case using a single site characterized by one frequency ω_B with a Lorentzian distribution (figure 2(*a*)). From the frequency distribution (figure

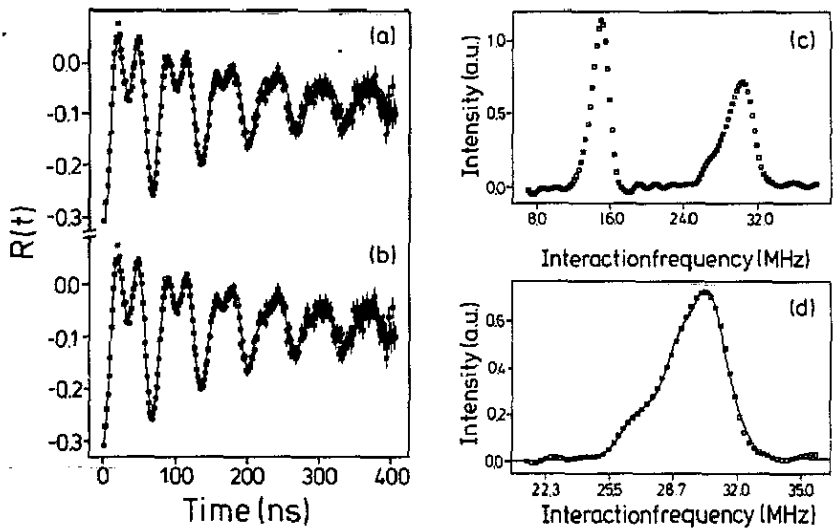

Figure 2. Magnetic hyperfine field distribution for ^{111}In–$Ni_{98.6}Al_{1.4}$ at room temperature: (*a*) the TDPAC precession pattern fitted with a single damped frequency; (*b*) represents the fit with four equally damped frequencies as indicated in frequency range (*c*); (*d*) the fit of the double-frequency domain of the Fourier transform (*c*) by a sum of four Lorentzian distributions, clearly indicating the four sites present.

2(*c*)), there is no doubt that satellites to the left of the main peak are present. A first indication of the number of satellites present and the values of their corresponding frequency shifts can be obtained by fitting the frequency distribution pattern with a sum of Lorentzian distributions (figure 2(*d*)). Indeed these satellites are also found at consistent positions in the fitting of the time spectrum (figure 2(*b*)). The satellites are nearly equidistant and well resolved but slightly broadened by a similar frequency distribution less than 1%. The numerical data obtained from least-squares fitting of the time spectra are collected in table 2 for different impurities. It should be stressed that, in the data analysis, the Fourier transforms and their fits are used as a guidance only and all conclusions are based solely on the TDPAC time spectra as given in figure 2(*b*) as an example. Indeed, the time spectrum is much more sensitive to frequency shifts than is the Fourier transform because the width $\Delta\nu \simeq 2$ MHz of lines in the latter is determined by the finite time window. This is illustrated in figure 3. The time spectrum in figure 3(*a*) is simulated using a main frequency of 15.6 MHz (the fraction equals 65%) and a satellite with a frequency shift of -0.80 MHz (fraction of 35%) both having the same and small distribution width of 0.16 MHz. The presence of this satellite is clearly visible in the time domain (i.e. changing shape in addition to the damping), but in the corresponding Fourier transform in figure 3(*b*) not resolved.

For the investigated alloys Ni–Al, Ni–V and Ni–Cr, the impurity concentration dependence was studied. A typical example is shown for the Ni–V case in figure 4. The computer fitting of the $R(t)$-curves gave the parameters indicated in tables 3, 4 and 5 respectively. The frequency values from those tables are plotted in figure 5 to show the general concentration dependence of each magnetic interaction frequency ν_i ($i = 0, 1, 2, 3, 4$) irrespective of the impurity type. Since the frequency component ν_0 should correspond to the magnetic hyperfine field at the Cd probe in an almost pure nickel

Table 2. Summary of the parameters obtained from fitting the magnetic precession pattern: c is the concentration, ν_i is the magnetic interaction frequency ν_B of the ith site, and A_i^E and A_i^B are the experimental and calculated populations in a sphere with coordination number $Z = 78$.

Impurity	c (at.%)	$\langle\delta\nu\rangle$ (MHz)	ν_0 (MHz)	A_0^E (%)	A_0^B (%)	ν_1 (MHz)	A_1^E (%)	A_1^B (%)
V	0.3	0.13(1)	15.55(3)	84(2)	78	14.6(2)	13(1)	20
Al	1.4	0.10(1)	15.37(6)	33(2)	33	14.74(6)	35(1)	37
Cr	2.3	0.13(2)	14.71(9)	22.2(8)	16	13.6(2)	26.4(8)	30
ν_2 (MHz)	A_2^E (%)	A_2^B (%)	ν_3 (MHz)	A_3^E (%)	A_3^B (%)	ν_4 (MHz)	A_4^E (%)	A_4^B (%)
13.8(3)	3(1)	2	—	—	—	—	—	—
14.02(9)	20(1)	21	13.15(9)	12(1)	8	—	—	—
12.6(2)	26.4(8)	27	11.4(2)	16.6(8)	16	10.2(2)	8.5(7)	7

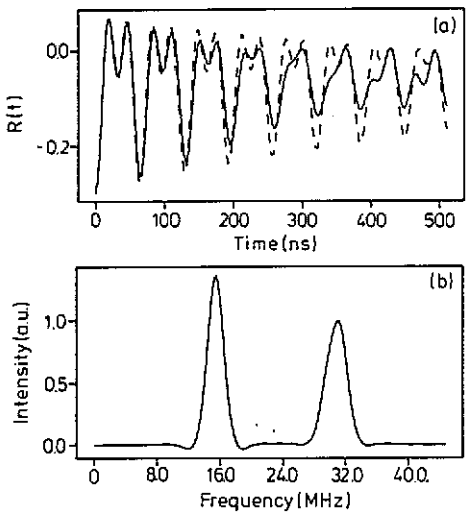

Figure 3. (*a*) Simulated magnetic time spectrum including two frequencies, shifted by −0.80 MHz, with the same distribution width of 0.16 MHz (———) and the magnetic spectrum without a frequency shift (– – –); (*b*) the corresponding Fourier transform of the two-frequency time spectrum.

environment, indeed linear extrapolation of ν_0 to zero concentration gives 15.66(3) MHz, while the slope is −0.39(2) MHz (at.%)$^{-1}$. This frequency value corresponds almost exactly to the pure Ni value, as expected.

For all alloys studied in this work, the populations A_i^E deviate from the statistical probability to find m impurities in a particular shell around the probe. For an alloy with impurity concentration c, we would expect

(i) the probability to find one impurity in a certain shell proportional to the coordination number of that particular shell and

(ii) the probability in a certain shell to decrease with increasing number of impurities.

Neither of these tendencies could be found in our experimentally determined populations.

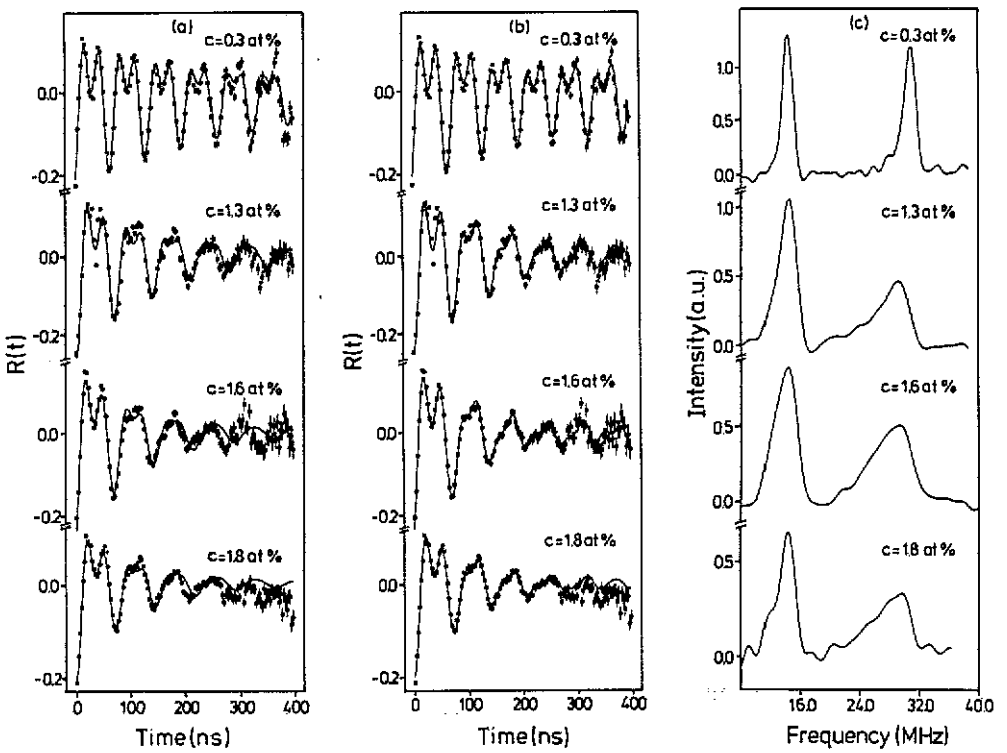

Figure 4. Magnetic hyperfine field distribution of room-temperature measurements on ^{111}In–Ni–V at four solute concentrations: (*a*) TDPAC spectrum fitted with a single damped frequency; (*b*) time spectrum fit containing multiple satellites; (*c*) Fourier-transformed TDPAC spectra.

Table 3. Derived parameters for Ni–Al as a function of concentration. (E, experimental; B, binomial within a sphere of Z atoms).

c (at.%)	$\langle\delta\nu\rangle$ (MHz)	ν_0 (MHz)	A_0^E (%)	A_0^B (%)	ν_1 (MHz)	A_1^E (%)	A_1^B (%)
0.5	0.35(8)	15.4(2)	73(13)	68	14.2(6)	27(10)	27
0.8	0.14(2)	15.4(1)	57(2)	54	14.6(2)	32(3)	34
1.4	0.10(1)	15.37(6)	33(2)	33	14.74(6)	35(1)	37
3.0	0.24(5)	15.3(2)	43(5)	9	14.3(3)	33(4)	22

ν_2 (MHz)	A_2^E (%)	A_2^B (%)	ν_3 (MHz)	A_3^E (%)	A_3^B (%)	ν_4 (MHz)	A_4^E (%)	A_4^B (%)
—	—	—	—	—	—	—	—	—
13.5(3)	11(1)	10	—	—	—	—	—	—
14.02(9)	20(1)	21	13.15(9)	12(1)	8	—	—	—
13(1)	8(3)	27	12.3(6)	12(4)	21	17.8(9)	4(1)	—

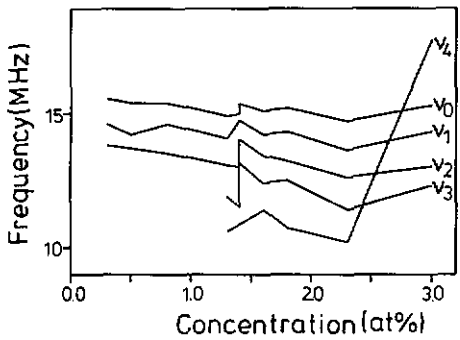

Figure 5. Graphical representation of all the data in tables 3–5 for the magnetic interaction frequencies ν_i ($i = 0, 1, 2, 3, 4$) as a function of impurity concentration.

Table 4. Derived parameters for Ni–V as a function of concentration.

c (at.%)	$\langle\delta\nu\rangle$ (MHz)	ν_0 (MHz)	A_0^E (%)	A_0^B (%)	ν_1 (MHz)	A_1^E (%)	A_1^B (%)
0.3	0.13(1)	15.55(3)	84(2)	78	14.6(2)	13(1)	20
1.3	0.18(2)	14.90(6)	34(2)	35	14.05(9)	30(1)	37
1.6	0.08(2)	15.09(9)	27(2)	27	14.2(2)	27(1)	36
1.8	0.30(3)	15.2(2)	22(3)	23	14.3(2)	34(2)	34

ν_2 (MHz)	A_2^E (%)	A_2^B (%)	ν_3 (MHz)	A_3^E (%)	A_3^B (%)	ν_4 (MHz)	A_4^E (%)	A_4^B (%)
13.8(3)	3(1)	2	—	—	—	—	—	—
13.05(9)	20(1)	19	11.9(2)	12(1)	7	10.6(3)	4.6(6)	2
13.4(2)	22(1)	23	12.4(2)	16(1)	10	11.4(2)	7.6(7)	3
13.2(3)	26(2)	25	12.5(3)	13(1)	12	10.73(3)	4.8(9)	4

Table 5. Derived parameters for Ni–Cr as a function of concentration.

c (at.%)	$\langle\delta\nu\rangle$ (MHz)	ν_0 (MHz)	A_0^E (%)	A_0^B (%)	ν_1 (MHz)	A_1^E (%)	A_1^B (%)
1.4	0.22(2)	15.0(2)	31(2)	33	14(2)	34(2)	37
2.3	0.13(2)	14.71(9)	22.2(8)	16	13.6(2)	26.4(8)	30

ν_2 (MHz)	A_2^E (%)	A_2^B (%)	ν_3 (MHz)	A_3^E (%)	A_3^B (%)	ν_4 (MHz)	A_4^E (%)	A_4^B (%)
13(2)	25.6(8)	21	11.5(2)	9.5(9)	8	—	—	—
12.6(2)	26.4(8)	27	11.4(2)	16.6(8)	16	10.2(2)	8.5(7)	7

The population A_0^E, corresponding to the frequency ν_0, can be compared with the population A_0^B calculated assuming a binomial distribution. The probability of finding no impurities among Z neighbouring atoms is given by $A_0^B = (1-c)^Z$, with c the impurity concentration and Z the 'coordination number' of the cluster considered. Surprisingly, for Al, V and Cr impurities the best agreement between experimental A_0^E-values and calculated A_0^B-values is obtained by disregarding the discrete-shell structure, but using the coordination number $Z = 78$. This suggests that the observed fraction of probes sensing the interaction frequency ν_0 corresponds to no X impurities within a sphere of five shells around the probe. Furthermore, a close correspondence exists between the measured relative populations of all satellites and the probability calculated using

$$A_n^B = [Z!/n!(Z-n)!]c^n(1-c)^{Z-n}$$

assuming $n = 1, 2, 3, \ldots,$ X impurities among the atoms contained within the five nearest shells (78-atom cluster) (table 2). This observation is further supported by the concentration-dependent measurements, given in tables 3–5, below 3 at.% impurity concentration (see the 3 at.% Al case).

Obviously a highly non-random impurity distribution is observed around an In atom but resulted in a few distinguished In–X configurations only. The latter statement is concluded from well defined satellite lines observed in our TDPAC spectra, in contrast with the frequency distribution expected from a random population of all impurity configurations possible in a 78-atom cluster. The relative amplitudes of the observed peaks and their dependence on impurity concentration lead to the conclusion that all the impurity atoms otherwise statistically contained in five nearest-neighbour shells surrounding the In probe are involved in the creation of magnetic satellites. In this sphere of 78 atoms the impurity–impurity interaction is such that only distinct localization of these impurities is possible. Usually, however, the location of impurities, as a result of repulsive or attractive interactions, may be governed by a periodic potential of Blandin–Deplanté [10] type. Our evidence suggests that a particular shell around the In probe is preferentially populated with impurities, creating only a few well defined geometric configurations for the In–multiple X clusters.

4.3. Discussion

In the present study the Al, Cr, V impurity–probe configurations are found to be well defined and formed within a distinct nearest-neighbour shell around the In probe from the following arguments.

(i) From quadrupole interaction results above the Curie temperature no near-neighbour probe–impurity close pairs were observed. Because of the short range of the quadrupole interaction, the small interaction strength observed in the non-cubic site was attributed to impurity configurations in the third or further shells around the probe.

(ii) The distinct frequencies measured in the magnetic spectrum appear with almost equal and rather small distribution width (average value of 0.12(2) MHz); thus they are well defined.

(iii) The large population of the left wing frequencies in the distribution pattern (figure 2(*c*)) excludes the presence of various configurations formed from randomly distributed impurities in a five-shell sphere around the Cd probe. On the contrary, because of the almost equally spaced, well resolved hyperfine field satellites, rather unique impurity configurations are suggested, behaving as multiples of a basic configuration. If impurity perturbations are independent of each other and additivity in

local moment perturbation is assumed [11], equidistant satellite hyperfine fields then are expected to be due to the configurations of one, two, three, . . . X impurities in the same neighbour shell around the probe.

Unfortunately our data give no evidence to support any of the geometrical structures possible for multiple impurities in the same shell. Although one may expect that, while the position of the satellite mainly depends on the number of impurities in the 'trapping' shell, their geometrical configuration may eventually be reflected in the respective shifts. Of course one may argue that the quadrupole interaction depends more sensitively on the geometry of the impurity cluster. However, because of the small quadrupole interaction frequency observed, a distribution of this frequency may not be too conclusive or reliable. Indeed the assumption of a model for impurity collection in a particular shell, say the third shell, allows a model-dependent fit of the quadrupole interaction spectra measured above T_C. Instead of the already mentioned (section 4.1) 'two-site' fit, we try a 'four-component' fit consisting of

(i) a pure nickel environment (constant anisotropy) and
(ii) three fractions of equation (2) type for quadrupole interaction.

In order to test our model, we allow some freedom in the fitting of the relative populations of the different sites as well as in the respective interaction frequencies. The starting value of these parameters were inferred from the satellite populations in the magnetic spectra and the three site frequencies were multiples of a basic interaction frequency, the latter corresponding to the EFG induced by one impurity in, for instance, the third-nearest-neighbour shell. Because we expect the configuration to be well defined, no frequency distributions were allowed. The result is quite satisfactory, in that very good quality of the fit is obtained for values not essentially different from those expected. Of course this argument does not prove the model but simply shows its consistency with the data, because the same Ni–Al spectrum can be fitted almost equally well assuming just a single site with a finite interaction frequency $eQV_{zz}/h = 2.84(6)$ MHz and a distribution of 0.35 MHz.

Finally, the question arises whether the presence of the small but finite quadrupole interaction influences the conclusions from the magnetic spectra. The magnetic hyperfine field will be along the easy axis of magnetization, which for nickel is the ⟨111⟩ direction. An impurity in the third shell induces an EFG oriented along the ⟨211⟩ directions, making angles $\beta = 19.47°, 61.87°$ and $90°$ with multiplicity 6, 12 and 6, respectively. Because the quadrupole interaction strength is very small relative to the magnetic interaction ($\omega_Q/\omega_B \simeq 5 \times 10^{-3}$), we apply a diagonal approximation for the interaction Hamiltonian $H = H_M + H_Q$. In such a case, the observed interaction frequencies per site are given by the expression

$$N\omega_B \pm n\omega_Q P_2(\cos\beta)$$

with $N = 1$ or 2 and $n = 6$ or 12 and 18. Because in a cubic lattice the average value $\langle P_2(\cos\beta)\rangle = 0$, to first order, the quadrupole interaction induces only a slight broadening on the magnetic frequencies. Indeed, a rigorous calculation using the full Hamiltonian shows that the magnetic interaction frequency will be observed with an enhanced distribution width, due to the quadrupole interaction, of nearly 0.7% in the present situation.

In conclusion, the main observations are as follows.

(i) The quadrupole interaction measurements show a strong repulsive probe–impurity interaction, indium expelling the Al, V, Cr impurities from the first-nearest-neighbour shell around the probe.

(ii) The magnetic hyperfine field distributions show well defined satellite structures and correspond to configurations built with one, two, three, . . . X impurities in the same nearest-neighbour shell. The impurities involved originate from trapping within a sphere containing 78 atoms (five nearest-neighbour shells) around the In probe.

(iii) The observed satellite hyperfine fields which thus originate from impurities beyond the second-nearest-neighbour shell are reduced in absolute value relative to the pure matrix hyperfine field value.

Acknowledgments

The authors are grateful to Professor K Krolas (Cracow, Poland) for stimulating discussions. This work was financially supported by the Belgian Interuniversitair Instituut voor Kernwetenschappen.

References

[1] Samoilov B N, Sklyarevskii V V and Stepanov E P 1959 *Sov. Phys.–JETP* **36** 448
[2] Budnick J I, Burch T J, Skalski S and Raj K 1970 *Phys. Rev. Lett.* **24** 511
[3] Van Der Woude F and Sawatzky G A 1974 *Phys. Rep.* **12** 335
[4] Niculescu V A, Burch T J and Budnick J I 1983 *J. Magn. Magn. Mater.* **39** 223
[5] Wichert Th and Recknagel E 1986 *Microscopic Methods in Metals* XVI, ed U Gonser (Berlin: Springer) p 317
[6] Hrynkiewicz A Z and Krolas K 1983 *Phys. Rev.* B **28** 1864
[7] Arends A R and Pleiter F 1982 *Hyperfine Interact.* **12** 143–65
[8] Decoster P, De Doncker G, Hrynkiewicz A Z and Rots M 1990 *Hyperfine Interact.* **60** 845–8
[9] Krolas K 1981 *Phys. Lett.* **85A** 1097
[10] Blandin A and Deplanté J L 1962 *J. Phys. Radium* **23** 609
[11] Shavishvili T M and Kiliptari L G 1979 *Phys. Status Solidi* b **92** 39